Experimental Study on Vertical and Lateral Bearing Characteristics of Rock-Socketed Long Piles at Deeply Backfilled Sites in Nuclear Power Engineering

Liqin Ding *, Tao Lv , Liwei Chen , Xuhong Wang , Libo Chu

Posted Date: 23 April 2026

doi: 10.20944/preprints202604.1602.v1

Keywords: bearing capacity; pile foundation; in-situ experiment; backfill soil; nuclear engineering

 doi:10.20944/preprints202604.1602.v1

Article

Experimental Study on Vertical and Lateral Bearing Characteristics of Rock-Socketed Long Piles at Deeply Backfilled Sites in Nuclear Power Engineering

Liqin Ding *, Tao Lv, Liwei Chen, Xuhong Wang and Libo Chu

Beijing Institute of Nuclear Engineering, China Nuclear Power Engineering Co., Ltd, Beijing 100840, China

* Correspondence: dlq891@163.com; Tel.+86010-88573871

Abstract

The foundation of nuclear power plants is special as large-scale earth filling is often required. The properties of the backfill soil differ significantly from naturally deposited soils with regard to deformation and bearing capacity. For pile foundations, a thick backfill layer near the top may change the bearing mode around the pile. In this paper, parallel multi-pile tests were conducted to thoroughly investigate the vertical and horizontal bearing characteristics of long rock-socketed piles at backfill nuclear site. The results show that longer piles tend to have higher vertical bearing capacity, however, they do not necessarily exhibit smaller displacements when subjected to vertical load. When the applied vertical load increases, the effect of end resistance of piles becomes more pronounced, meanwhile, deeper soil layers exert a more significant impact on the axial forces within the pile body. Short piles with more part in backfill layer may endure a hoop tightening effect at the upper part of the pile, resulting in very little frictional resistance being provided by the lower soil. At the vertical load level preceding failure, the distribution of axial force and shaft resistance along the pile length will change. The typical mechanism of transition from static to dynamic friction between soil and piles that lead to shaft resistance is more apparent for longer piles but inhomogeneous soil like backfill layer will make the transition complex. When subjected to lateral loading, piles with better integrity show more pronounced elastic features, smaller maximum horizontal displacement and less residual horizontal displacement. The selection of the proportional coefficient for determining piles' horizontal bearing capacity should correspond to the specific load and displacement. The results and in-depth analysis of the piles' bearing capacity will provide intuitive experience for the analysis of pile foundations, thus offer valuable references for the design and construction in similar engineering.

Keywords: bearing capacity; pile foundation; in-situ experiment; backfill soil; nuclear engineering

1. Introduction

Pile foundations are widely used in human engineering projects. Designers commonly have confidence by using piles to support the foundation of buildings due to the piles' good environmental adaptability, strong load-bearing capacity and mature construction techniques. However, when buildings have higher displacement requirements or the geological conditions around the piles are complex, the application of piles may be limited. Hence, mastering the bearing capacity and safety margin of pile foundations under specific geological conditions is of great importance for designers.

The straightforward and reliable way to determine the bearing capacity of piles is to conduct in-situ tests. Many references have reported on the tests of vertical bearing capacity of piles. Kou et al. [1] conducted a series of field tests to investigate the behavior of open-ended prestressed high-strength concrete (PHC) pipe piles installed into clay. The distribution of residual forces after

 doi:10.20944/preprints202604.1602.v1

installation and the effect on the bearing capacity were discussed in detail. Pham et al. [2] gathered lots of pile static load test results and used random forest algorithms to analyze the results. It shown that the average SPT (Standard Penetration Test) value and pile tip elevation were both important for prediction of vertical bearing capacity. Zhang et al. [3] presented a field study on the axial behavior of four large-diameter piles combined with tip-and-side post grouting. It was concluded the bearing capacity were significantly affected by the quantity of pressurized cement slurry and the mechanical properties of the soil surrounding the shaft. Yan et al. [4] conducted model tests to study the influence of different red clay water content and different compaction degrees on the bearing characteristics of pile foundations. The results indicate that increasing the compaction degree or reducing the moisture content has a more significant effect on increasing the side resistance. Wei et al. [5] carried out a series of pile tests and analyses to evaluate the vertical bearing capacity of rock-socketed piles and to investigate their mechanical characteristic and load-bearing behavior. Based on the test data, the pile axial force, frictional resistance, and load-sharing ratio were calculated and analyzed. Yang et al. [6] conducted in-situ vertical load field tests on two bored piles and analyzed the load transfer mechanics.

Due to specific requirements of buildings and structures, some literature also focused on experimental research on the horizontal bearing capacity of pile foundations. Bai et al. [7] tested six rock-socketed bored piles in the field to investigate the lateral bearing characteristics of rock-socketed bored piles in silty clay formations in coastal areas. Two lateral loading tests in which the pile lengths are 5.2 m and 11.07 m were carried out by Liu et al. [8] to investigate the difference of rigid pile and flexible pile. Besides, some researchers also focused on the effects of artificial soil layers. A series of centrifuge tests were performed by Taghavi et al. [9] to investigate the behavior of laterally loaded pile groups in improved and unimproved soft clay. Faro et al [10] also conducted a series of laterally loaded pile tests both in natural ground and in cemented treated soil. Kang et al. [11] used gravel soil with different contents of crushed stone to replace the natural soft soil to study the horizontal bearing capacity of pile foundation through single pile tests. Huang and Li [12] studied the effects of displacing hard shell on the horizontal bearing characteristics of pile foundation in layered soft soil. The influences of the thickness and the shear strength index of the replaced hard-shell layer are analyzed. Yang [13] studied the applicability and reinforcement effects of layered grouting technic in soil on the horizontal bearing capacity of pile foundation.

In addition to experimental methods, there are theoretical and empirical methods as well as numerical method to determine bearing capacity of pile foundations. For example, the Chinese Code (JGJ94-2008) [14] illustrates an empirical method to calculate the vertical bearing capacity of piles embedded in common soil layers. Besides, the calculation methods for horizontal bearing capacity of single pile and pile groups based on the *m*-method are also introduced in this Code. Several empirical methods were illustrated by Mishra et al. [15] to predict the vertical compressive ultimate load of rock-socketed piles. The *p*-*y* curve method is applied by American Petroleum Institute Code [16] to calculate the horizontal bearing capacity of piles. Based on numerical method, Seol et al. [17] proposed that two-dimensional elastoplastic finite element analysis was suitable for estimating the load transfer and coupling effects of piles. Gutierrez-Ch et al. [18] suggested that the DEM could be used to reveal the key behaviors of the load-settlement response, lateral resistance and pile-rock interface damage of rock-socketed piles. Besides, Machine learning algorithms [19] are also used to predict piles' bearing capacity. However, if condition permit, in-situ testing remains the most reliable approach, particularly under complex geological conditions.

Currently, nuclear power develops fast in China. Nuclear projects are generally large in scale and requiring substantial earthwork during site formation. Thick backfill soil often appears as surface layer of soils at nuclear power plant site, which introduce more uncertainties in the application of pile foundations. Therefore, it is essential to study the bearing capacity levels, influencing factors and mechanisms of these pile foundations under such conditions. Besides, comprehensive study on vertical and horizontal in-situ tests of long piles are rarely seen in literature. This becomes the primary motivation of this paper. In this work, the engineering and site conditions are firstly introduced. Then, the vertical and lateral loading test methods are described in detail, including the test scheme and

 doi:10.20944/preprints202604.1602.v1

data monitoring. Finally, the measured results are thoroughly interpreted, including the influences of soil layers around the pile, soil layer distribution and characteristics of pile body on the bearing capacity of piles. The results and conclusions will have significant reference value for similar engineering designs and constructions.

2. Overview of the Tests

2.1. Engineering Background

The test site for this experiment is located at the Qinshan nuclear power plant in southeast of Zhejiang Province, China. The purpose of the test is to evaluate the reliability of the dry storage facility for spent nuclear fuel in the plant when using pile foundations. The building covers an area of approximately 4,740 square meters and is used to store about 65 concrete storage blocks for spent fuel, each with a mass of approximately 200t. The foundation of the building bears significant vertical loads and eccentric loads.

A notable characteristic of this building is its location in an artificially filled area, which belongs to a coastal land reclamation geomorphological unit. The artificial backfill layer is thick (with average thickness of 10.5m), non-uniform and has poor engineering properties, significantly differing from naturally deposited soils. The backfill layer primarily consists of fragmented and blocky stones from mountain excavation and dumping, with extremely poor sorting. The block sizes vary greatly, typically ranging from 3 to 10cm, with the largest exceeding 60cm. The lithology mainly comprises slightly weathered to unweathered pyroclastic rocks filled with clay. The backfilling activity was completed 10 years ago. Groundwater in the region is mainly present as Quaternary pore water, with a water table depth of 7~9m. Beneath the backfill layer, there are relative thick Quaternary soil layers before bedrock. Prior to conducting pile foundation tests, a site investigation was carried out, during which soil samples were obtained from 26 boreholes and subjected to laboratory testing to determine mechanical parameters. The vertical distribution and primary properties of each soil layer are shown in Table 1. In this table, SZH1~SZH6 are the six test piles. The thicknesses of each soil layer around each pile are also shown.

Table 1. Stratification and parameters of soil for each tested pile.

Layer	Soil Description	Thickness for Each Pile (m)						ω (%)	γ (kN/m³)	c (kPa)	φ (°)	E_{s1-2} (MPa)
		SZH1	SZH2	SZH3	SZH4	SZH5	SZH6					
①	Backfill soil	14.4	15.5	19.2	20.5	7.5	7.8	/	19.0	0~2	36~38	30.0
③1	Silty Clay	10.4	7.5	4.3	3.5	17.5	17.4	31.2	18.6	15.8	8.2	3.5
③2	Clay	1.7	1.5	1.2	1.3	12.0	11.8	38.7	18.0	14.0	5.8	4.0
③3	Breccia	1.7	2.3	3.0	3.2	0	0	/	/	/	/	/
④	Silty Clay	11.0	7.3	5.5	5.0	15.8	15.6	26.3	19.5	43.6	15.1	10.5

2.2. Pile Configuration

The detailed information of the test piles is shown in Table 2. Similar to actual design of the building, the test piles are cast-in-place piles with a diameter of 1m. The piles are rock-socketed with the tips embedded approximately 1m into the moderately weathered bedrock. The lengths of piles SZH1 to SZH4 are approximately 35 to 40m, while the lengths of SZH5 and SZH6 are around 55m. The concrete strength grade of the pile body is C45. Ordinary Portland cement as well as mineral admixtures such as fly ash and silica fume was used. The pile body is reinforced with 20 longitudinal steel bars, each with a diameter of 22mm and made of HRB400 steel. The longitudinal steel bars are mechanically connected. Spiral stirrups are installed along the pile body, with a spacing of 100mm within the densified zone near the pile top and 200mm in lower zone. The thickness of the concrete cover for the reinforcement is 60mm. The overall steel reinforcement replacement rate of the pile is 0.968%.

 doi:10.20944/preprints202604.1602.v1

Table 2. Details of the tested pile.

Pile No.	Test method	Diameter	Total Length	Concrete Grade	Reinforcement
SZH1	Vertical loading	1.0 m	40.18 m	C45	
SZH2	Horizontal loading	1.0 m	35.50 m	C45	Main steel bar:
SZH3	Vertical loading	1.0 m	35.67 m	C45	20Φ22
SZH4	Horizontal loading	1.0 m	35.17 m	C45	Steel ratio:
SZH5	Vertical loading	1.0 m	54.98 m	C45	0.968%
SZH6	Horizontal loading	1.0 m	54.73 m	C45	

3. Test Plan and Data Monitoring

3.1. Monitoring System

The monitoring system mainly consists of the following components:

(1) Load measurement system. The applied load signal in both vertical and lateral directions are transmitted to the static loading instrument via pressure sensors connected to the hydraulic jacks. The model of the pressure sensor is ST3000LBCIIERY.

(2) Displacement measurement system. In vertical loading, the settlement monitoring position at the pile top is approximately 0.2m below the pile head. Four displacement sensors are installed symmetrically on the pile body in two mutually perpendicular directions. In horizontal loading, two horizontal displacement monitoring systems are set up at the ground level and 50cm above the ground (near the pile top) to measure displacements at the two positions. For each position, two displacement sensors are symmetrically installed on both sides of the test pile within the plane of force action. The model of all displacement sensors is RS-WS50. Additionally, during the horizontal loading test, inclinometer tubes are pre-installed inside the test piles. The inclinometers (model TL-06B) are used to measure the horizontal displacement at different pile sections to obtain the deflection curves.

(3) Pile internal force (strain) measurement system. Intelligent string-type steel bar strain sensors (model JMZX-422HAT) are pre-embedded at predetermined cross-sections of pile along with the construction of reinforcement cage. In the vertical loading, before loading and after each load step stabilizes, an instrument (model JMZX-3001L) is used to read the strain values of the gauges. Based on the strain values, the axial forces at different positions along the pile body can be calculated. For the vertically loaded pile SZH1, the arrangement of strain gauges along the pile body is shown in Figure 1(a). In the lateral loading, the strain gauges are symmetrically arranged in the cross section on the tension and compression bars far from the neutral axis. Within the main load-bearing portion (upper section of the pile), the sensors are densely spaced at 1m intervals. Beyond this depth, the spacing increases to 2m, and no sensors are installed below 20m depth. For the horizontally loaded pile SZH2, the arrangement of strain gauges along the pile body is shown in Figure 1(c). The layout of strain gauges in the cross-sections of the vertically and laterally loaded piles is shown in Figure 1(b).

 doi:10.20944/preprints202604.1602.v1

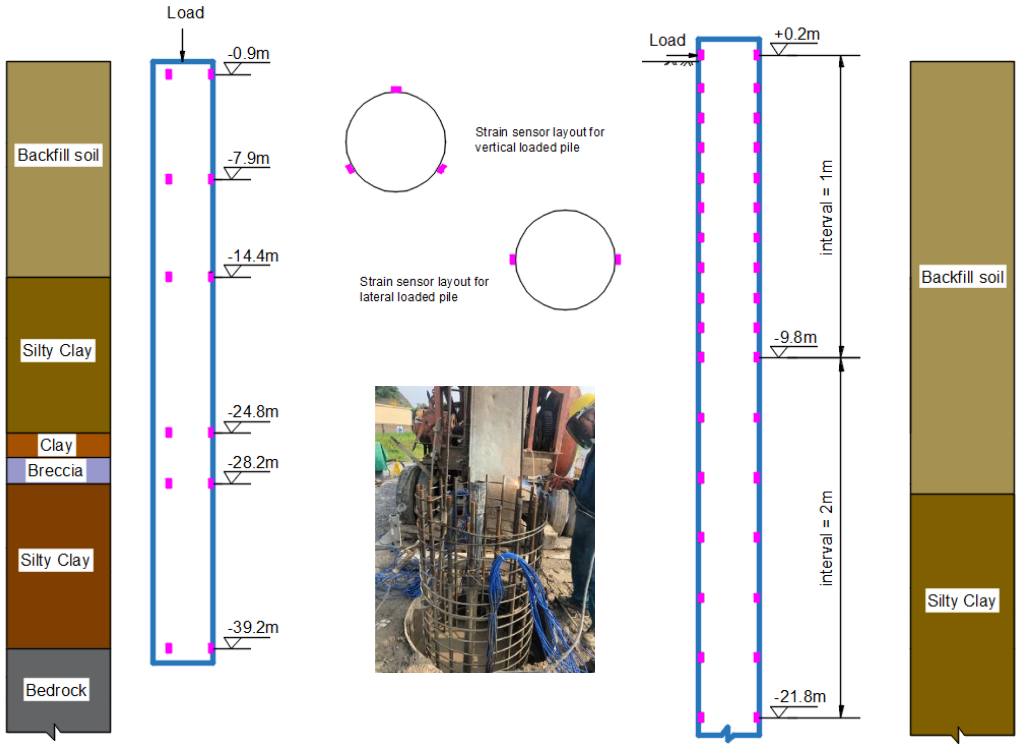

(**a**) (**b**) (**c**)

Figure 1. Sensor configuration on the test pile: (**a**) on the vertical loaded pile SZH1; (**b**) layout on cross-section and field installation; (**c**) on the horizontal loaded pile SZH2.

3.2. Vertical Loading Scheme

The vertical loading tests were conducted on three test piles, namely SZH1, SZH3, and SZH5. The configuration of the piles is shown in Table 2. The vertical force was provided by a weight platform, with a flatbed stacking platform measuring 12.0m×12.0m. The stacking material consisted of prefabricated blocks. The main beams of the stacking platform were composed of two parallel steel beams sized 12.0m×1.07m×0.5m. Secondary beams were made up of ten steel beams sized 12.0m×0.7m×0.5m. The secondary beams were placed on pre-stacked blocks, with the reaction force generated by jacks pushing against the underside of the main beams. A schematic diagram of the loading setup is shown in Figure 2(a), and the on-site stacking arrangement is shown by Figure 2(c).

The slow-maintained load method was employed. Each stage load was 2000kN before reaching the maximum load value. After applying each stage load, the settlement at the pile head was measured at 5min, 15min, 30min, 45min, and 60min intervals. Subsequent readings were taken every 30 minutes. Loading was stopped when signs of instability in the pile appeared or when the predetermined maximum load value (24000kN) was reached. Unloading then proceeded in stages, with each unloading stage being twice of that during loading.

According to monitoring plan, the axial force of the pile can be calculated by:

$$Q_i = \sigma_{s,i} A_s + \sigma_{c,i} A_c = \varepsilon_{s,i} E_s A_s + \varepsilon_{c,i} E_c A_c , \quad (1)$$

in which Q_i is the axial force of the pile at the *i*-th cross-section, A_s and A_c, $\sigma_{s,i}$ and $\sigma_{c,i}$, $\varepsilon_{s,i}$ and $\varepsilon_{c,i}$, E_s and E_c are the section area, stresses, strains, elastic modulus for steel bars and concrete, respectively. Considering the bond between steel and concrete, there is $\varepsilon_{s,i} = \varepsilon_{c,i}$.

 doi:10.20944/preprints202604.1602.v1

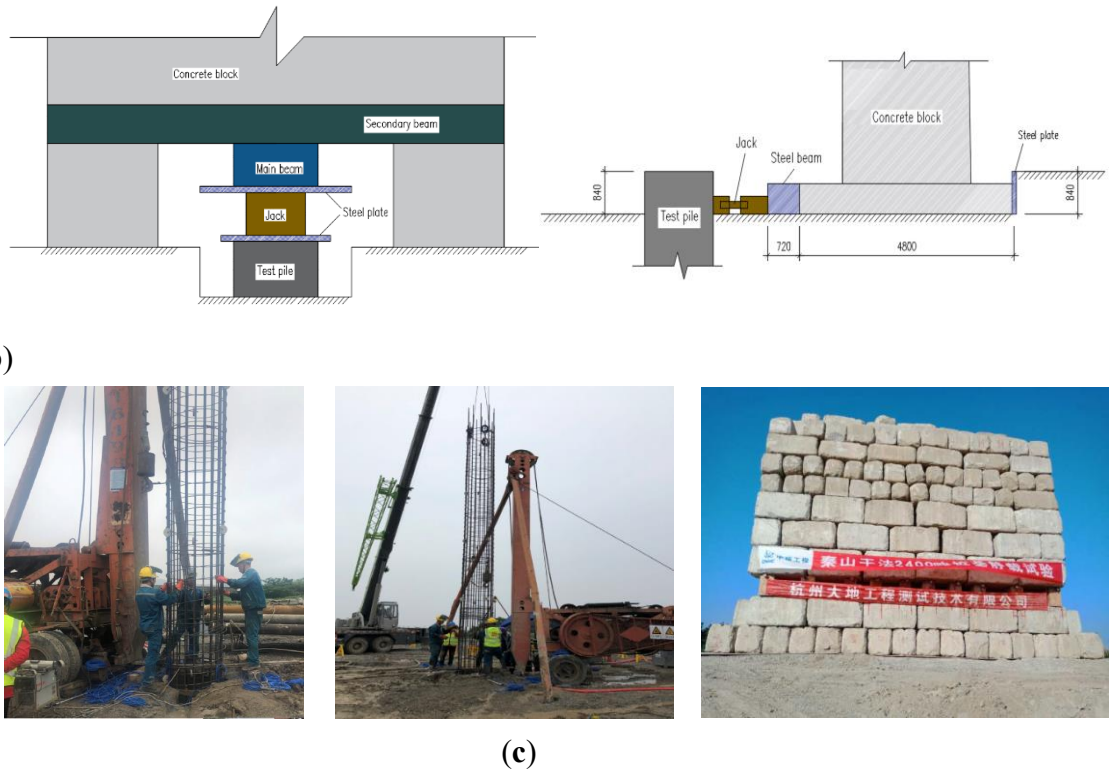

Figure 2. Static load test set-up for single pile: (**a**) schematic illustration of vertical loading device; (**b**) schematic illustration of horizontal loading; (**c**) pile construction and loading blocks in field.

3.3. Horizontal Loading Scheme

The lateral loading tests were conducted on piles SZH2, SZH4, and SZH6, with the pile configurations shown in Table 2. The test utilized a reaction system, as illustrated in Figure 2(b). The test reaction force was provided by stacking prefabricated concrete blocks with a hydraulic jack. The action point of the horizontal force was at ground level. A spherical hinge seat was installed at the contact point to ensure the jack's force could be applied horizontally through the pile's axis.

The load was applied incrementally in equal stages, with each stage load being 1/10 of the maximum loading value, i.e., 65kN. Based on the experience from the SZH2 pile, subsequent tests used slightly larger load intervals. After applying each load stage, the displacement at the pile head was measured at 5min, 15min, 30min, 45min, and 60min intervals. Subsequent readings were taken every 30 minutes, with each stage being observed for a period of 120min to 240min. Loading was stopped if excessive horizontal displacement or pile damage occurred. Unloading then proceeded in stages, with each stage being 2 to 3 times of the loading.

The section moment of the pile can be calculated using the following formula based on the test values from the embedded sensors:

$$M = \frac{E_0 I_z (\varepsilon_t - \varepsilon_c)}{b_0}, \tag{2}$$

where M represents the bending moment at the measured cross-section, E_0 is the elastic modulus of the reinforced concrete, ε_t and ε_c are the strains on the tension and compression sides of the section, respectively, b_0 is the distance between the sensors on the tension and compression sides.

3.4. Low-Strain Testing

Considering the horizontal bearing capacity of the pile foundation may be affected by the integrity of the pile, low-strain reflection wave tests on piles SZH2, SZH4, and SZH6 were conducted prior to horizontal loading tests. During testing, an elastic compression wave is generated by

 doi:10.20944/preprints202604.1602.v1

hammering at the top of the pile, which propagates downward along the pile at a wave speed *Vc*. When this wave encounters changes in cross-section or variations in the density of the pile material, it produces reflections and transmissions. The reflected signals are received by sensors installed at the top of the pile. Based on the processed time-domain waveform and wave speed, it is possible to determine whether there are defects in the pile, as well as their type, location, and severity.

4. Analysis and Discussion of Test Results

4.1. Vertical Loading Tests

4.1.1. Loading and Displacement Development

To facilitate the comparison and reveal more details, three test piles were selected for vertical bearing capacity tests, namely SZH1, SZH3, and SZH5, with lengths of 40.18m, 35.50m, and 54.98m, respectively. Figure 3 shows the load-displacement curves of these test piles under applied vertical loads. The vertical load was applied at the top of the piles, with loading increments of 2000kN and unloading increments of 4000kN, up to a maximum load of 24000kN. Overall, as the load increased, the pile head displacements of the three test piles gradually increased, and the rate of increase in displacement also grew with increasing load. In the early stages of loading, the slopes of the three curves were similar, indicating that their load-displacement characteristics did not differ significantly. This is because when the load is small, both the pile shaft and the surrounding soil are in the small-strain elastic stage and the pile-soil interface exhibits continuous and compatible deformation. As the load further increased, the load-displacement curves of the SZH3 and SZH5 piles became closer, while the displacement change of the SZH1 pile was relatively slower. The Q-s curves of the SZH1 and SZH5 piles did not show any abrupt changes; however, when the load on the SZH3 pile reached 24000kN, its displacement increased sharply, exhibiting clear signs of failure. Actually, for long piles subjected to very high vertical loads, both compressive strength failure and buckling failure may occur. The failure of pile SZH3 in this case is more likely a buckling failure and the post-buckling behavior of piles can be further investigated in future studies. Under the maximum applied load, the pile head displacements of the SZH1 and SZH5 piles were 32.45mm and 46.42mm, respectively. After unloading, the residual pile head displacements were 3.24mm and 20.56mm, respectively. Additionally, it can be observed that under each load level, the pile displacement of the SZH5 pile was greater than that of the SZH1 pile. Considering the pile lengths shown in Table 2, it is evident that under the same vertical load, longer piles do not necessarily have smaller pile displacements; this is also related to the distribution of soil layers and the inherent properties of the pile itself.

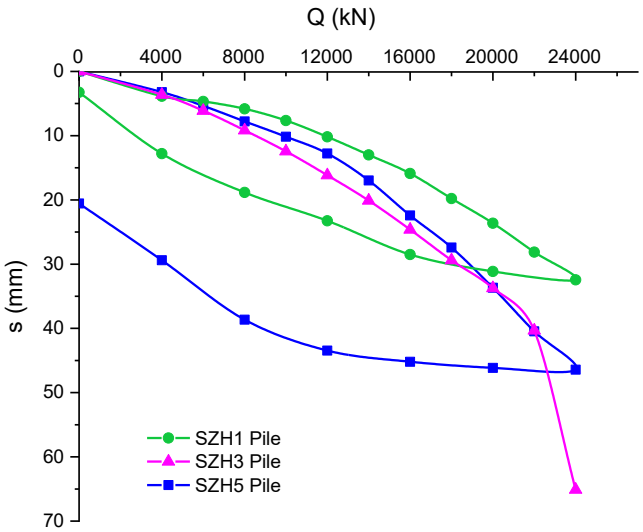

Figure 3. Q-s curves of three test piles subjected to vertical loads.

 doi:10.20944/preprints202604.1602.v1

4.1.2. Variation of Pile Axial Force

Sensors were pre-embedded on the reinforcing bars at different depths within the piles to measure the axial forces endured by different sections of the pile. Figure 4 shows the distribution of axial forces along the lengths of the SZH1, SZH3, and SZH5 piles when different loads are applied to the pile heads. It can be observed that, overall, the axial forces in the pile bodies decrease with depth, reflecting the influence of frictional resistance from the surrounding soils. When smaller loads are applied, the axial force at the pile toe is small, indicating that the base resistance plays a minor role at this stage. As the applied load gradually increases, the effect of end resistance becomes more pronounced. Generally, as the applied load increases, the axial forces within the pile body increase uniformly. But for longer piles (such as SZH5), this uniformity weakens near the pile toe. For example, the SZH5 pile beyond a depth of 40m, the slopes of all curves significantly decrease. This indicates a markedly increased influence of deeper soil layers on the axial forces. From this perspective, it can be concluded that under greater applied loads, deeper soil layers exert a more significant impact on the axial forces within the pile body. On the other hand, observing the curves of SZH3 pile reveals that even at the penultimate loading stage before failure (the applied load, AL=22MN), the axial force curve already shows a different trend from previous stages. This suggests a predictive indication of failure through changes in axial force. While the ultimate vertical bearing capacity can be more easily identified for the SZH3 pile due to its failure, the SZH1 and SZH5 piles did not reach a definitive ultimate bearing capacity. However, analyzing the patterns of change in the axial force curves, it can be seen that the curve for the SZH5 pile (Figure 4(c)) maintains a relatively uniform change even under high loads, whereas the curve for the SZH1 pile (Figure 4(a)) begins to show signs of change under very high loads (e.g., AL=24MN). This suggests that the actual ultimate vertical bearing capacity of the SZH5 pile may be higher than that of the SZH1 pile, highlighting the advantages of longer piles.

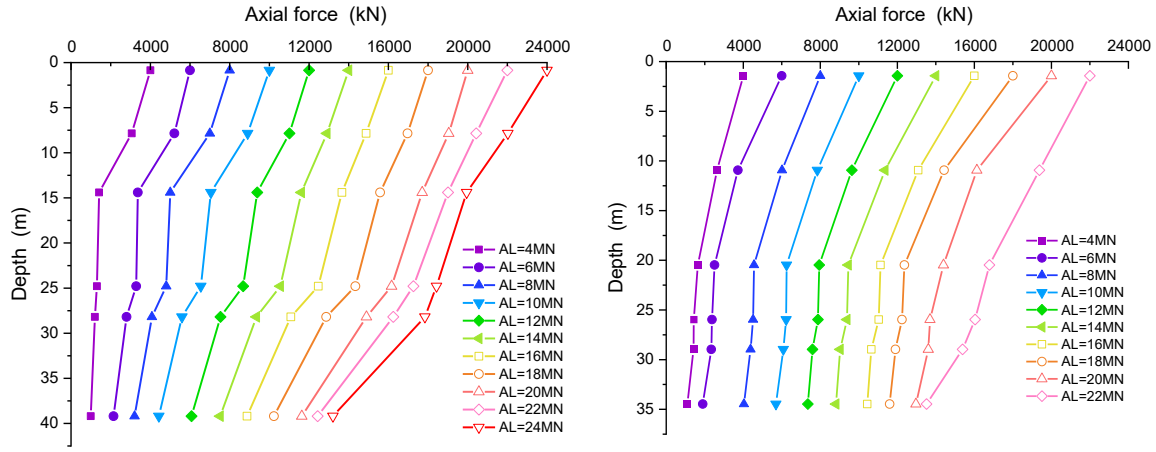

(a) (b)

 doi:10.20944/preprints202604.1602.v1

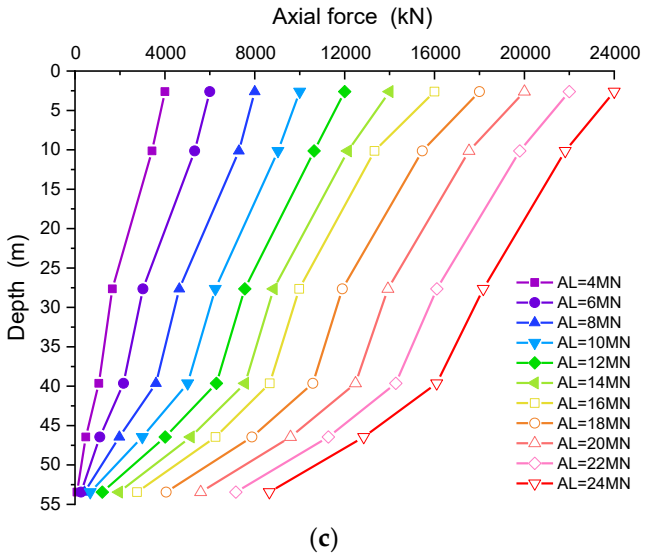

Figure 4. Axis force distribution along the pile of (**a**) SZH1, (**b**) SZH3, (**c**) SZH5 under different loads applied (AL) at the pile head.

4.1.3. Variation of Shaft Resistance

Figure 4 illustrates the variations of axial forces, which actually reflect the frictional effects of soils along the pile. To better analyze the influence of different soil properties on shaft resistance, Figure 5 shows the distribution curves of shaft resistance determined by calculating the differences in axial forces at adjacent cross-sections. It can be observed that the shaft resistance curve of the SZH5 pile in Figure 5(c) exhibits a similar pattern for different loads. However, for the SZH1 and SZH3 piles, the patterns of shaft resistance are quite different when larger loads are applied (e.g., AL=22~24MN). Based on the preceding analysis, this could be a precursor to insufficient vertical bearing capacity of the pile. This sign cannot be found in the Q-s curves.

In Figure 5(a), the depths from 0 to 14.4m are located within backfill layers. It can be seen as the applied load increases, the variation in shaft resistance is not uniform. This is likely due to the poor homogeneity of the backfill layer. Compared to the backfill layer, other soil layers exhibit more regular patterns, where shaft resistance generally increases with applied load, except when approaching the ultimate load. In Figure 5(c), these laws are clearer due to its greater bearing capacity. However, the situation for the SZH3 pile is quite different. Figure 5(b) shows a phenomenon where the upper backfill layer provides higher shaft resistance while deeper soil layers provide lower shaft resistance, contrary to the other two piles. From Tables 1 and 2, it is known the total lengths of pile SZH1, SZH3 and SZH5 are 40.18m, 35.67m and 54.98m, respectively, while the lengths in backfill layer are 14.4m, 19.2m and 7.5m, respectively. It is noted that longer piles with less part in backfill layer may lead to clear patterns of shaft resistance along the pile. On the contrary, short piles with more part in backfill layer may result in that most of the shaft friction of piles occurring within the backfill layer. For example, for pile SZH3, the shaft resistance below 20m depth is quite small. This indicates that the inhomogeneous and relative stiff (fragmented and blocky stones) property of the upper backfill layer may lead to significant variations in the shaft resistance along the pile. This even creates a hoop tightening effect at the upper part of the pile, resulting in very little frictional resistance being provided by the lower soil. Pile SZH1 seems to behave as an intermediate state between Pile SZH5 and Pile SZH3. From the above analysis, it is found that when the thickness of uneven gravel-filled backfill layers is quite large, the distribution of shaft resistance along piles differs from that in uniformly layered soils. Using traditional empirical methods to determine shaft resistance may result in discrepancies.

 doi:10.20944/preprints202604.1602.v1

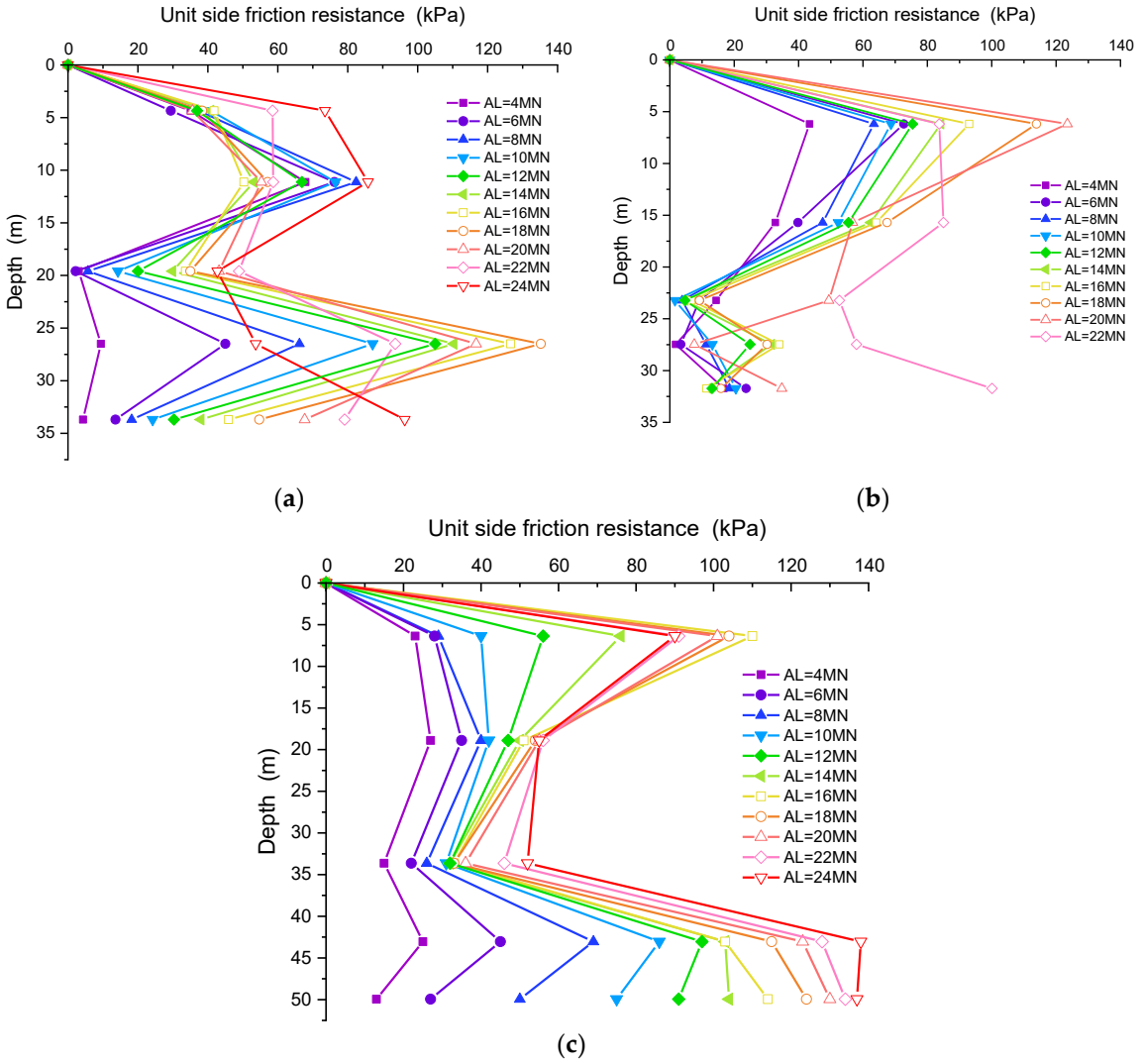

Figure 5. Shaft resistance distribution curve of different pile segments determined by the axial force difference: (a) pile SZH1, (b) pile SZH3, (c) pile SZH5.

4.1.4. Overall Change of Shaft and Base Resistance

The previous discussion elaborated on the distribution of shaft resistance in different soil layers. Figure 6 illustrates the evolution of overall shaft and base resistance of the three vertically loaded piles. It is noted all tested piles in this experiment were end-bearing piles with a rock-embedded depth of approximately 1m at the pile toe. It is clearly observed that for each test pile, both the shaft resistance and base resistance increase with the applied load. The curve patterns for the SZH1 and SZH3 piles are similar. When the applied load is small, the shaft resistance is larger than the base resistance. As the load increases, the base resistance gradually becomes more significant and eventually surpasses the shaft resistance. The critical load at which this transition occurs is higher for SZH1 than SZH3, indicating that the SZH3 pile exhibits base-bearing effects earlier. For the SZH5 pile, however, the shaft resistance remains greater than the base resistance regardless the applied load. This observation highlights that under similar geological conditions, increasing pile length significantly enhances the frictional effect of the surrounding soil on the pile, thereby somewhat diminishing the end-bearing effect.

From the perspective of base resistance ratio, it can be seen that all test piles exhibit a consistent trend. That is the base resistance ratio increase linearly with the applied load, showing a strong regularity. However, there are differences: the final base-bearing ratios for the SZH1 and SZH3 piles are around 55% to 61%, whereas the final base-bearing ratio for the SZH5 pile is only 36%. This holds

 doi:10.20944/preprints202604.1602.v1

true throughout the loading process. It further underscores the impact of pile length on the base-bearing ratio—the longer the pile, the smaller the base-bearing ratio.

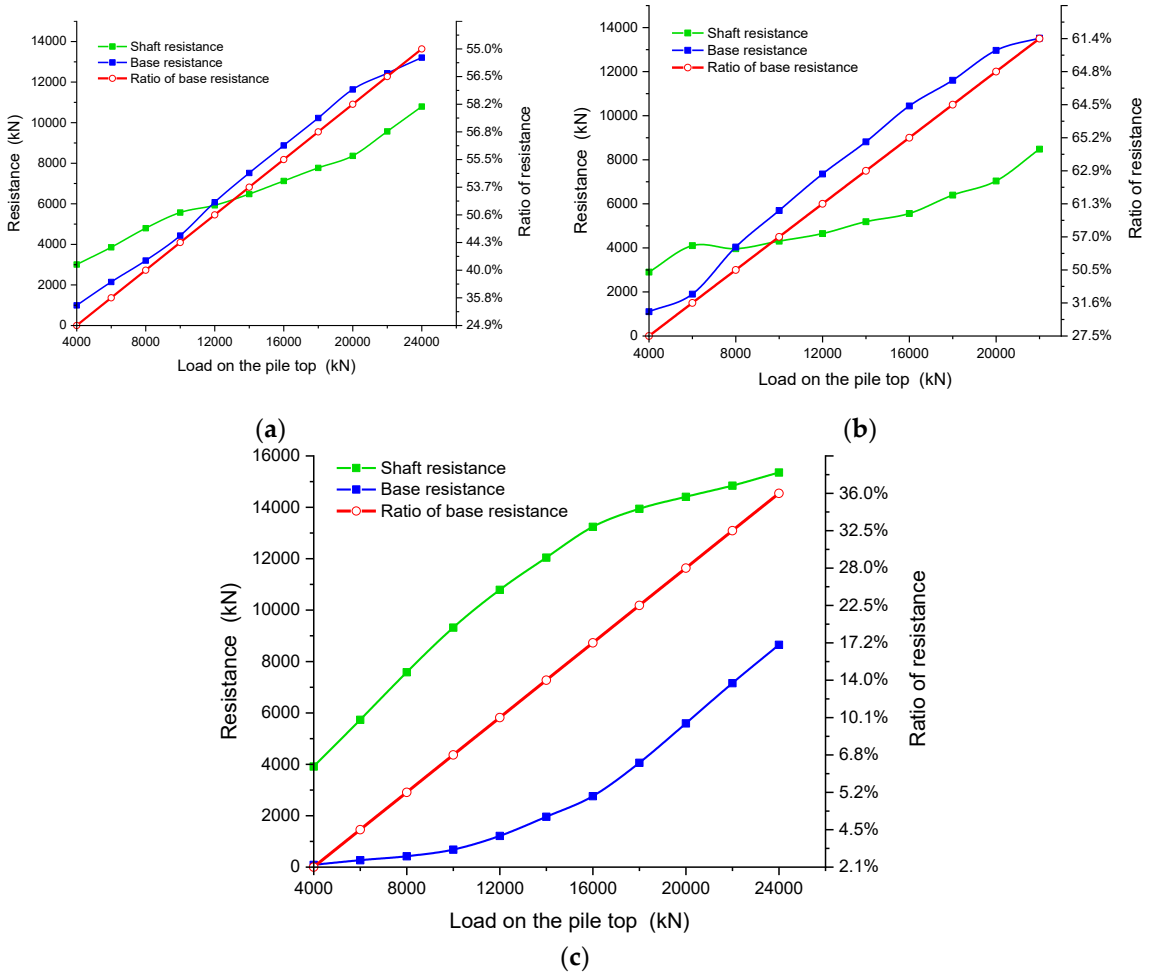

Figure 6. Evolution of total shaft resistance and base resistance of three vertical loaded piles: (a) SZH1, (b) SZH3, (c) SZH5 as the applied load increases.

4.1.5. Mechanism of Shaft Resistance Activation

The shaft resistance of a pile is generated by the friction effect between the pile and the surrounding soil. That is, when a vertical load is applied at the top of the pile, there tends to be relative displacement between the pile and the surrounding soil, thus creating either static or dynamic frictional side resistance at the pile-soil interface to hinder relative movement. The results shown in Figure 7 illustrate this mechanism quite intuitively. As shown in Figure 7(c), for longer piles like SZH5 (with a length of about 55m), as the applied load increases, the transition from static to dynamic friction between the pile and soil becomes very apparent. As to deep soil layers within the depth range of 39.6~53.5 m, when the applied load is small and causes minimal relative displacement, the side frictional resistance of the pile sharply increases. When the side friction reaches a certain point, it shows a turning point where it gradually stabilizes and develops steadily with increased displacement. This exemplifies the typical mechanism of transition from static to dynamic friction. As to shallower soil layers, such as silty clay and clay within the depth range of 10.1~39.6 m, similar patterns of change are also observed. The difference is that the static friction growth is slower, and the ultimate steady dynamic friction provided is smaller. Big difference appears in the upper backfill soil layer, where the shaft resistance generally shows an initial increase followed by stabilization with displacement. But it is challenging to clearly demonstrate the transition mechanism between static and dynamic friction. This means within non-uniform backfill layers, the variation of shaft resistance on piles becomes more complex. On the other hand, for shorter piles as shown in Figures 7(a) and (b),

 doi:10.20944/preprints202604.1602.v1

it can be seen that the overall curve changing pattern is basically consistent with that of longer piles. That is, a rapid increase in shaft resistance initially followed by stabilization. However, difference appears for Pile SZH3. It is seen failure due to insufficient bearing capacity occurs in the later stage, which is manifested on the curve as a rapid increase in shaft resistance. Through axial force analysis, it is deduced that Pile SZH1 may also have a tendency towards failure during this stage, leading to similar phenomenon in some of the curves. Additionally, Breccia layers containing shell fragments and characterized by poor uniformity appear in the soil around Piles SZH1 and SZH3, which has a certain disturbing effect on the development of the curves. These findings will help greatly for analyzing the development of shaft resistance in various types of soil layers.

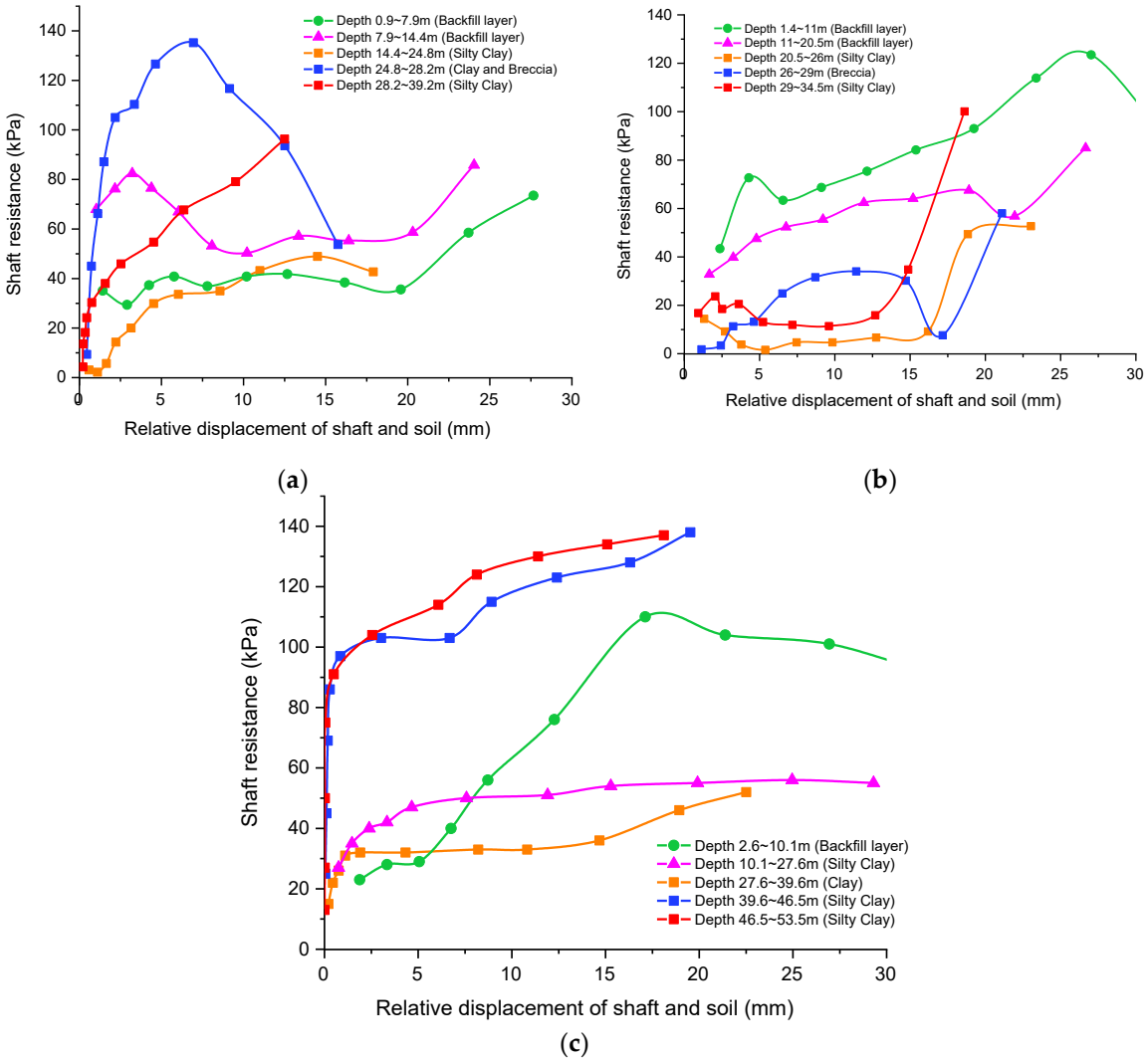

Figure 7. Relative displacement of shaft and soil and the induced shaft resistance along the pile of: (a) SZH1, (b) SZH3, (c) SZH5.

4.2. Horizontal Loading Tests

4.2.1. Pile Integrity Tests

Before conducting the horizontal loading tests, the RS-1616K(S) type dynamic testing instrument was used to perform low-strain pile integrity testing. The measured time-domain signal waveform diagrams of test piles SZH2, SZH4 and SZH6 are shown in Figure 8. As can be seen from the figures, the overall conditions of the diagrams for each pile are similar, with the waveform initially jumping near the top of the pile and no apparent second jump near the bottom of the pile. This is because the piles are rock-socketed. Further comparison reveals that the waveform from pile SZH2 is regular, with a clear wave train and no interface reflection within the pile body and the average wave velocity

 doi:10.20944/preprints202604.1602.v1

is relatively high. In contrast, the regularity of the waveform in the upper part of piles SZH4 and SZH6 is somewhat reduced, with a corresponding decrease in average wave velocity. According to the results of the low-strain testing, it is concluded pile SZH2 has better pile body integrity while piles SZH4 and SZH6 have slight defects in the upper part of the pile body. These results may have a certain impact on the horizontal bearing capacity of the piles.

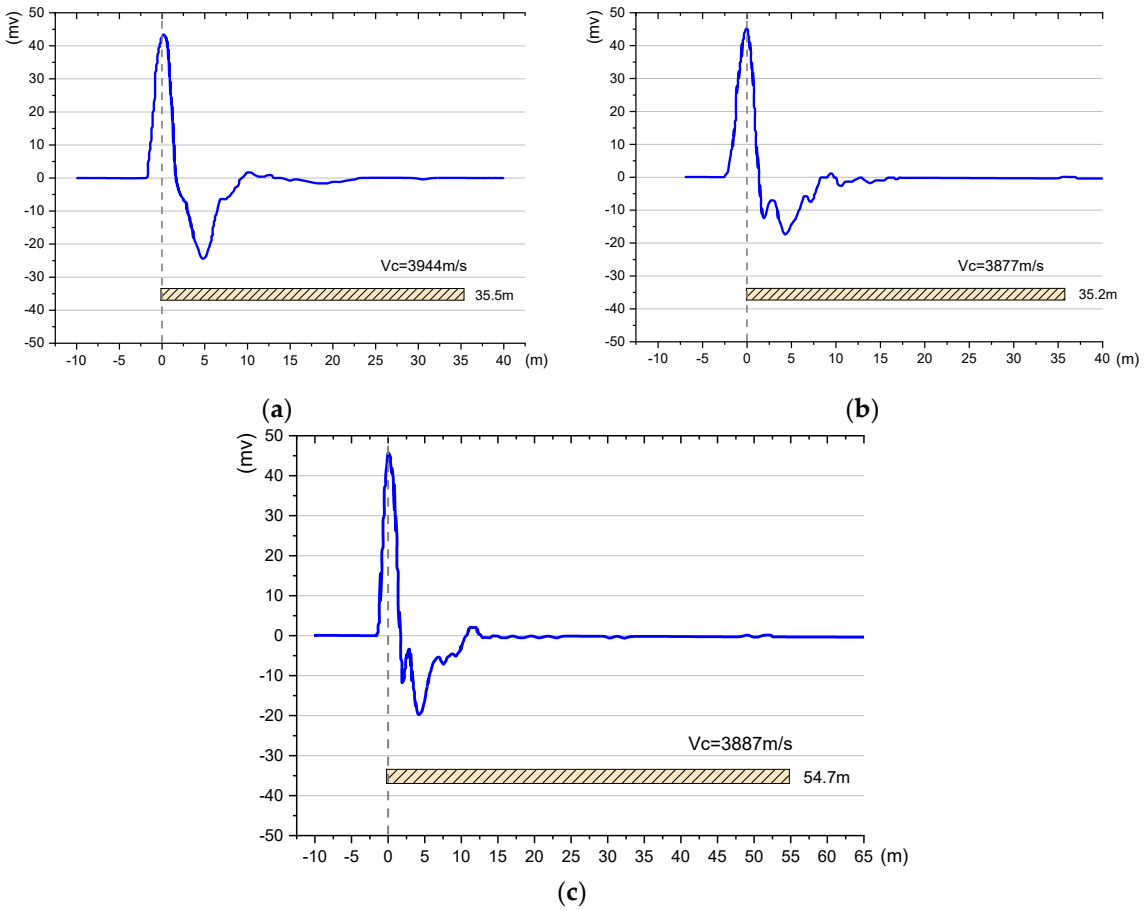

Figure 8. Time-domain signal waveform diagrams of measured piles: (a) SZH2, (b) SZH4, (c) SZH6.

4.2.2. Load-Displacement Curves

In the horizontal loading tests, three piles SZH2, SZH4, and SZH6 were set up for comparative experiments with lengths of 35.50m, 35.17m, and 54.73m, respectively. Given that the conditions of the three piles are similar except for their lengths, a smaller load increasing interval was adopted on pile SZH2 during the loading process. After obtaining basic experience, the load interval increased for tests on piles SZH4 and SZH6. Two horizontal displacement monitoring positions were set up in the tests: at the top of the pile and at the loading point where horizontal force is applied. As shown in Figure 2(b), the distance between the two positions is 0.5m.

Figure 9 shows the H-Y_0 curves under the action of forces applied to each pile. The results of both monitoring positions are presented, covering the processes of loading and unloading. From the H-Y_0 curves, it can be seen that the horizontal displacements basically increase with loading and decrease with unloading. The residual horizontal displacement of pile SZH2 after unloading is about 30mm, which is less than that of piles SZH4 and SZH6 (approximately 60mm and 43mm, respectively), even though the former was subjected to greater maximum loads. Moreover, the maximum horizontal displacement experienced by pile SZH2 is significantly smaller than the other two piles. Additionally, the H-Y_0 curve of pile SZH2 exhibits better linear characteristics. These phenomena may be related to the integrity test results of the piles previously conducted, indicating that piles with better integrity show more pronounced elastic features. Figure 9 also displays the H-$\Delta Y_0/\Delta H$ curves showing the rate of change of horizontal displacement. It is seen the displacement

 doi:10.20944/preprints202604.1602.v1

rate of the piles tends to increase in the early stage of loading. During this process, phenomena such as cracking of the pile body cause sudden changes in the growth rate. Unlike the latter two piles, after reaching its maximum displacement rate, pile SZH2 experiences a reduction in displacement rate and then maintains relatively stable within certain load ranges. This indicates that piles with better integrity exhibit higher toughness.

The critical load and ultimate load of the pile's horizontal bearing capacity can also be determined from the results in Figure 9. According to the relevant specifications of Code [20], the critical load can be determined by two methods. The first option is to take the previous load level before the appearance of an inflection point on the H-Y_0 curve. The second option is to take the load corresponding to the first inflection point on the H-$\Delta Y_0/\Delta H$ curve. For pile SZH2 in Figure 9(a), an obvious inflection point appears on the H-Y_0 curve when loaded to 520kN, while other inflection points are not evident. Besides, there are two clear inflection points on its H-$\Delta Y_0/\Delta H$ curve, corresponding to 325kN and 520kN. Therefore, the critical load of pile SZH2 is determined to be 325kN. For piles SZH4 and SZH6 shown in Figures 9(b) and (c), no clear inflection points are visible on their H-Y_0 curves, but there are two distinct inflection points on their H-$\Delta Y_0/\Delta H$ curves. Both the first inflection points correspond to a load of 260kN, which can be judged as the horizontal critical load of piles SZH4 and SZH6. According to the Code [20], the ultimate load for horizontally loaded piles can be determined by three methods. The first option is to take the horizontal load corresponding to the starting point of a significant drop on the H-Y_0 curve. The second option is to take the horizontal load corresponding to the second inflection point on the H-$\Delta Y_0/\Delta H$ curve. The third option is to take the previous load level before the pile breaks or the steel yields. However, the first phenomenon has not been found in the obtained curves and significant failure has not occurred either. Based on the preceding analysis, the second inflection points on the H-$\Delta Y_0/\Delta H$ curves can easily be identified from the test results shown in Figure 9. Therefore, it can be determined that the ultimate horizontal bearing capacities of piles SZH2, SZH4 and SZH6 are all 520kN.

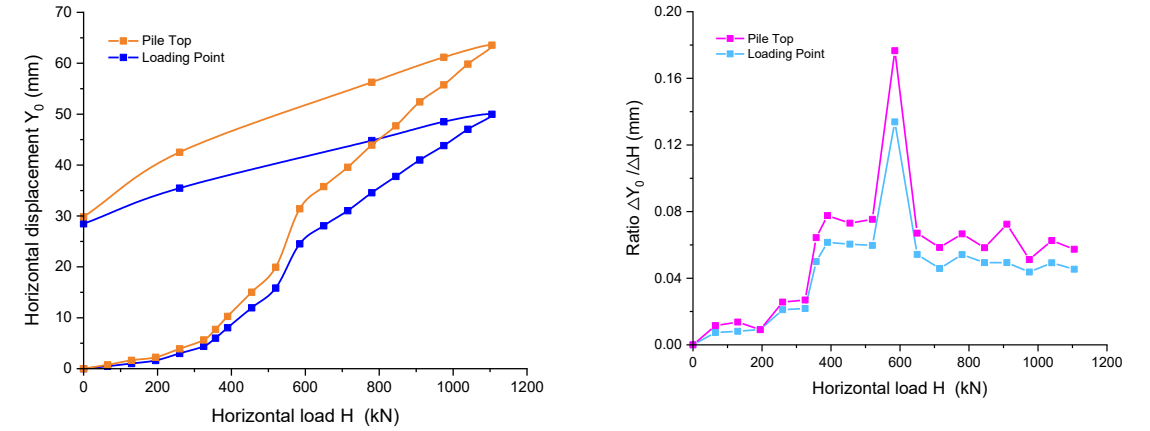

(a)

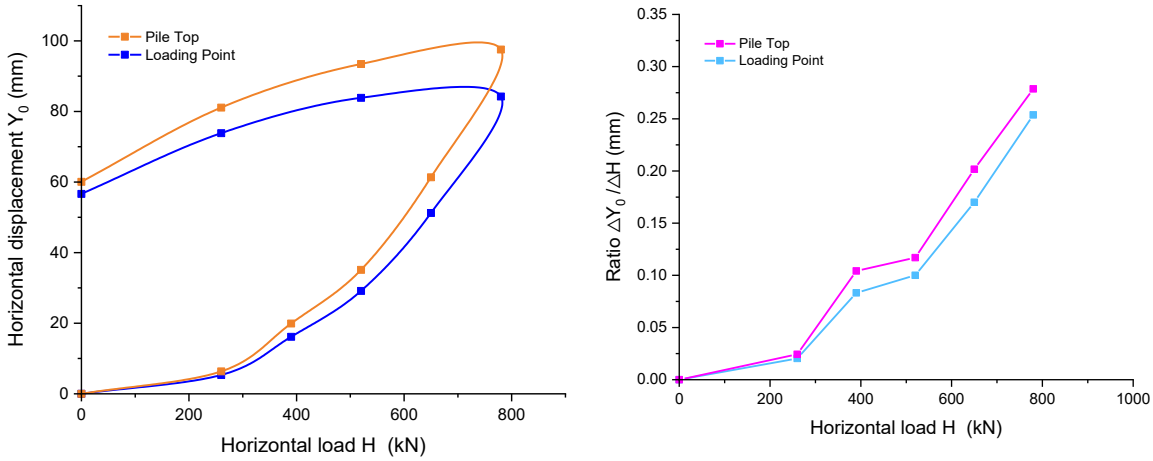

 doi:10.20944/preprints202604.1602.v1

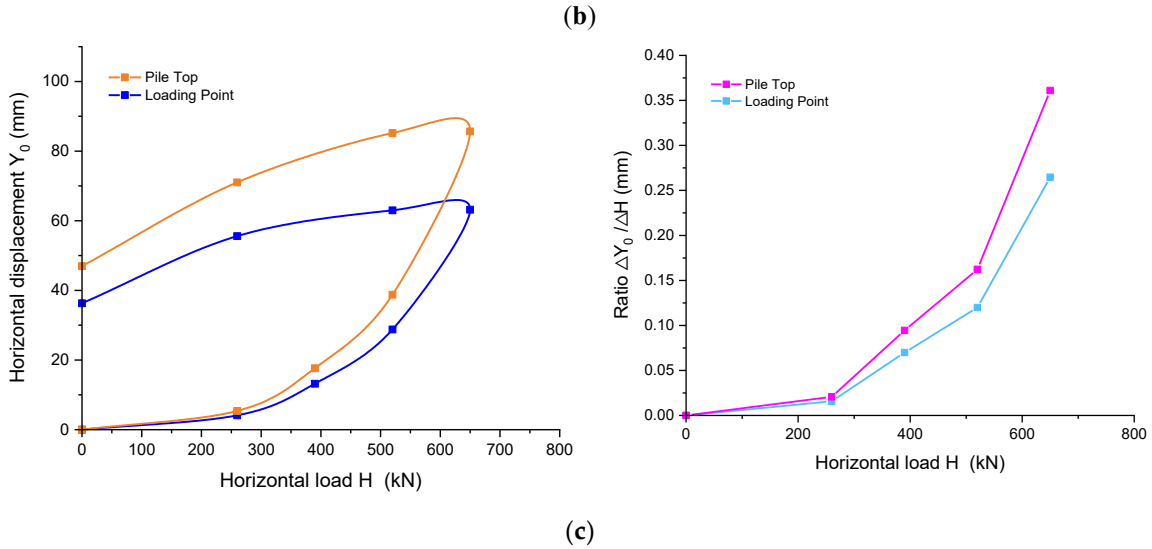

Figure 9. *H-Y₀* and *H-ΔY₀ /ΔH* curves for horizontal loaded piles: (a) SZH2, (b) SZH4, (c) SZH6.

4.2.3. Bending Moment and Deflection

Figure 10 shows the variation of pile bending moment with depth as the horizontal load increases. It can be seen that regardless of the magnitude of the applied load, the pile's bending moment shows a pattern of first increasing and then decreasing with depth. The maximum bending moment appears at a depth of 2~3m from ground. As the load increases, the maximum bending moment of the pile also gradually increases. The bending moment of SZH2 exists within the depth of 8m, while that of SZH4 and SZH6 exists within the depth of 9~10m. Besides, under the same load, the maximum bending moment of pile SZH2 is relatively larger. For instance, when AL=520kN, the maximum bending moment of pile SZH2 reaches 1430kN·m, while those of piles SZH4 and SZH6 are only 857kN and 666kN, respectively. This indicates that the soil around pile SZH2 has a relatively weak reduction effect on its bending moment. In contrast, the soils around the other two piles have a significant impact on their bending moments, with the degree of reduction effect reaching approximately 50%. The reason for this phenomenon should be related to the horizontal displacement of the pile body. That is, the greater the displacement, the more significant the influence of the soil around the pile belonging to passive zone. This could be explained by the subsequent deflection curves of the piles.

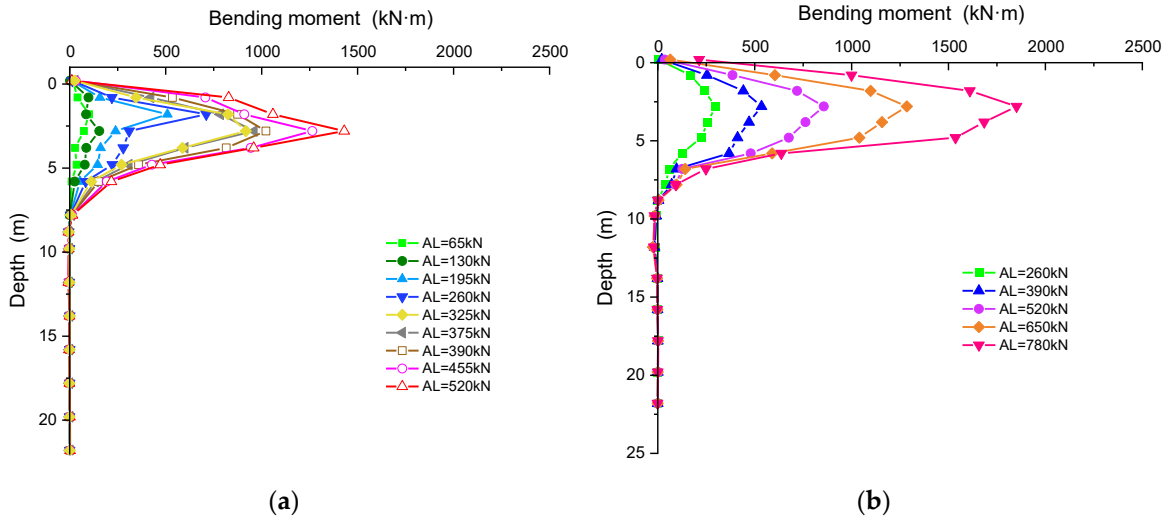

 doi:10.20944/preprints202604.1602.v1

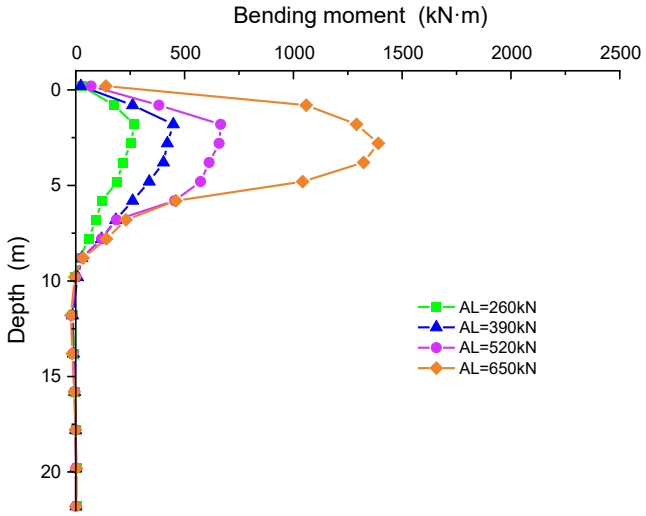

(c)

Figure 10. Variation of shaft bending moment with depth as the applied horizontal load increases: (a) pile SZH2, (b) pile SZH4, (c) pile SZH6.

Figure 11 shows the deflection curves of each pile along the depth direction as the load gradually increases. It shows that the deflection near the top of each pile gradually increases with the load, but the deflection at deeper positions varies significantly. For the SZH2 pile, when a horizontal load less than 260kN is applied, displacement occurs in the direction of the force (positive direction) at the pile head, and there is virtually no displacement below 5m depth. However, when the horizontal load reaches 325kN or more, positive displacement occurs within 3m from the top, while negative displacement occurs below 3m, acting as an elastic pile. In contrast, for the SZH4 and SZH6 piles, as the applied horizontal load gradually increases, the displacements of the piles are all positive. In theory, when the pile length is longer (e.g. SZH6 pile), the piles should exhibit better elastic characteristics under horizontal loads, which is contrary to the facts. This may due to the pile integrity results. According to Figure 8, the upper part of the SZH4 and SZH6 piles have some degree of formation defects, which leads to their semi-rigid characteristics under horizontal loads. Besides, it can be seen that under the same load, the displacement of the SZH2 pile is relatively smaller, while that of the SZH4 or SZH6 piles is larger. For example, when a horizontal load of 520kN is applied, the horizontal displacement at the top of the SZH2 pile is 13.7 mm, whereas the displacements of the SZH4 and SZH6 piles are 29.1 mm and 28.8 mm, respectively. Larger displacements at the top of the pile lead to greater reactive forces from the surrounding soil, which in turn affects the bending moment distribution of the pile body, explaining the phenomenon shown in Figure 11.

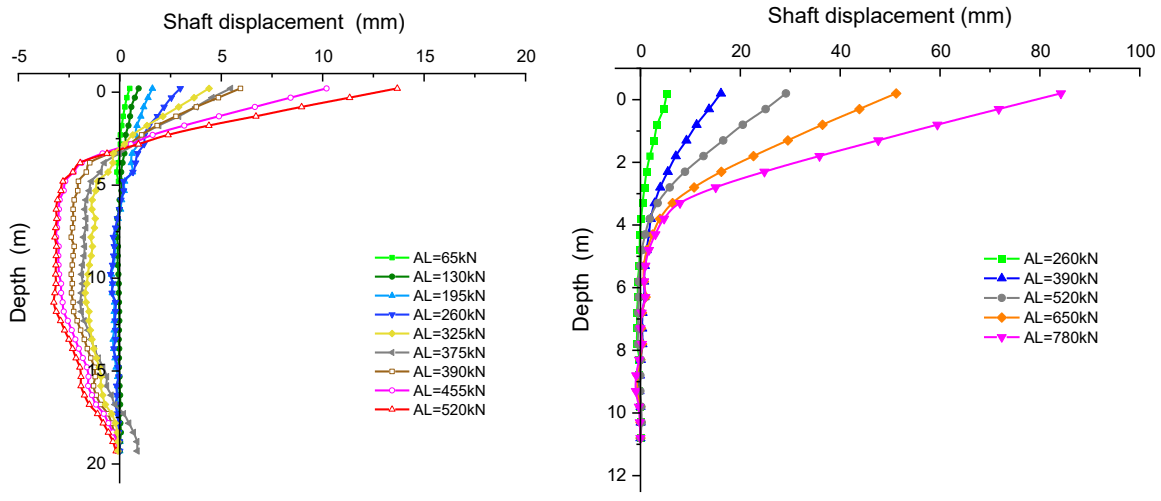

(a) (b)

 doi:10.20944/preprints202604.1602.v1

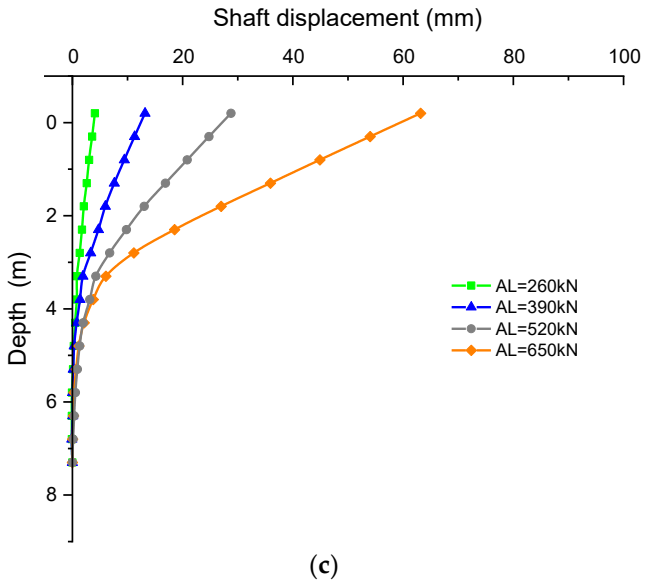

(c)

Figure 11. Variation of shaft bending moment with depth as the applied horizontal load increases: (a) pile SZH2, (b) pile SZH4, (c) pile SZH6.

4.2.4. Characteristic Value of Bearing Capacity

To determine the horizontal bearing capacity of piles, not only cracking or failures should be considered, but also need to consider engineering requirements, such as restrictions on displacement. For this purpose, another representative value for horizontal bearing capacity of piles appears, namely, the characteristic value. For instance, according to the Code (JGJ94-2008) [14], when the steel reinforcement ratio of cast-in-place piles exceeds 0.65%, 75% of the load corresponding to a horizontal displacement of 10mm at ground level (or 6 mm for sensitive buildings) can be taken as the characteristic value.

The H-Y_0 curves of three test piles within the loading range of 0~520kN are plotted on a single graph as shown in Figure 12. Calibration lines for the restrictive displacements of 6mm and 10mm are indicated. It can be observed that for horizontal displacements of 6mm, the corresponding horizontal loads for piles SHZ2, SHZ4 and SHZ6 are 357kN, 265kN and 285kN, respectively. Taking 75% of these values to determine the characteristic values as 268kN, 199kN and 214kN, respectively. Besides, when the horizontal displacement is limited to be 10mm, the corresponding horizontal loads are 422kN, 315kN and 340kN, respectively. Taking 75% of these values are 317kN, 236kN and 255kN, respectively. It can be seen despite different displacement limitation, the determined characteristic value for pile SHZ2 is significantly greater than the others. This indicates that for long rock-socketed cast-in-place piles, further increasing the pile length (such as pile SZH6) has minor impact on horizontal bearing capacity, whereas the integrity of the pile body (especially the upper part integrity) influences greatly.

 doi:10.20944/preprints202604.1602.v1

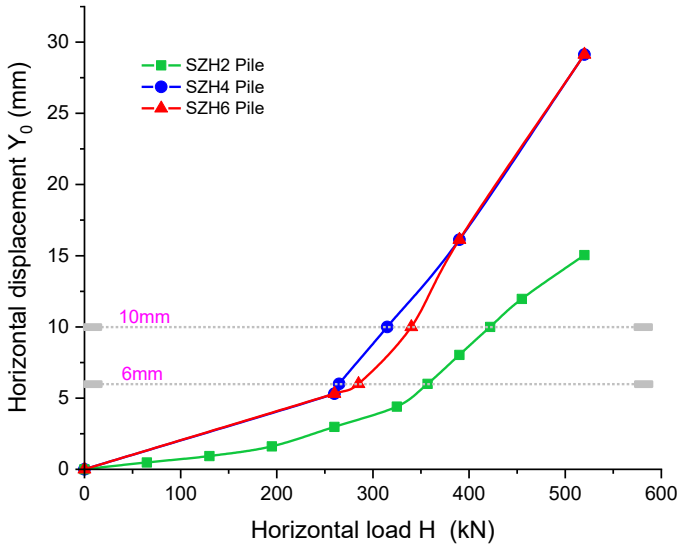

Figure 12. The *H*-*Y*₀ curves and the related characteristic values of horizontal bearing capacity.

4.2.5. Determination of Proportionality Coefficient m

Currently, the theoretical methods for determining the horizontal bearing capacity of piles are mainly divided into elastic methods, elastic foundation reaction methods, *p*-*y* curve methods, etc. Among these, the *m*-method, which assumes the reaction coefficient of foundation increases linearly with depth, is most widely used in the elastic foundation reaction method. This method shows good applicability for normally consolidated clay and sand under small deformation conditions, thus has been recommended in Code (JGJ106-2014) [20]. The *m*-method actually reflects the resistance of the surrounding soil to the horizontal displacement of the pile. In this section, we will analyze the value of proportionality coefficient *m* in this method based on the test results of three piles.

According to the specifications in Code [20], when estimating the characteristic value of the horizontal bearing capacity of a pile based on soil properties, the horizontal deformation coefficient of the pile α can be determined by Equation (3). Under conditions where the pile top is free and horizontal force acts at ground level, the *m* in Equation (3) represents the proportionality factor of the horizontal soil resistance coefficient around the pile, which can be determined by Equation (4).

$$\alpha = \left(\frac{mb_0}{EI}\right)^{1/5}, \tag{3}$$

$$m = \frac{\left(\frac{H}{Y_0} v_x\right)^{5/3}}{b_0 (EI)^{2/3}}, \tag{4}$$

in which $b_0$represents the calculated width of the pile shaft, $Y_0$is the horizontal displacement at the action point of horizontal force, *EI* is the bending stiffness of the pile shaft (for reinforced concrete piles, EI=0.85EcI_0, where *Ec*is the elastic modulus of concrete and $I_0$is the converted section inertia moment of the pile shaft, v_x can be determined based on the constraints at the top of the pile (for long piles with a free top, it can be taken as 2.441).

According to the measured results and Equation (3), the variation of *m* with increasing loads for three piles is calculated and shown in Figure 13. It can be seen that SZH2 was the first tested pile with a wider range of applied load and more detailed test results. Overall, the patterns of the three curves are similar, showing that the value of *m* gradually decreases with increased applied load. This aligns with previous experiences recorded in literature, indicating the *m* for the same pile is not constant but has a nonlinear relationship with the load. That is, at low load levels, the value of *m* is higher. As the load increases, the plastic zone of the soil around the pile gradually expands, leading to a decrease

 doi:10.20944/preprints202604.1602.v1

of the *m*. Therefore, the selection of the coefficient *m* should correspond to the actual load and displacement. In light of this situation, relevant literature suggests that for piles with a higher steel reinforcement ratio, the allowable displacement at the pile top and its corresponding load should be used to calculate the value of *m*. In Figure 13, the dashed lines indicate the *m* values calculated for each pile considering a limited displacement of 6mm at the pile top. It can be observed that the calculated *m* for piles SZH4 and SZH6 are 11.28MN/m^4 and 12.74MN/m^4, respectively. The results are close. Meanwhile, the calculated *m* for pile SZH2 is 18.54MN/m^4, significantly higher than the others. This difference actually verifies the impact of pile integrity on the determination of *m*, meaning that piles with better integrity will have larger *m*. The mechanism behind this could be understood as when the pile integrity is better, it is less prone to move, and smaller horizontal displacement corresponds to a larger *m* of the surrounding soil. This phenomenon highlights the significance of pile integrity for accurate determination of the *m* value. On the other hand, from Figures 9 and 10 it is known that the backfill layer has predominant influences on the horizontal bearing capacity of the piles. The measured *m* can serve as a reference for future projects as tests on thick backfill sites are rarely seen in literature.

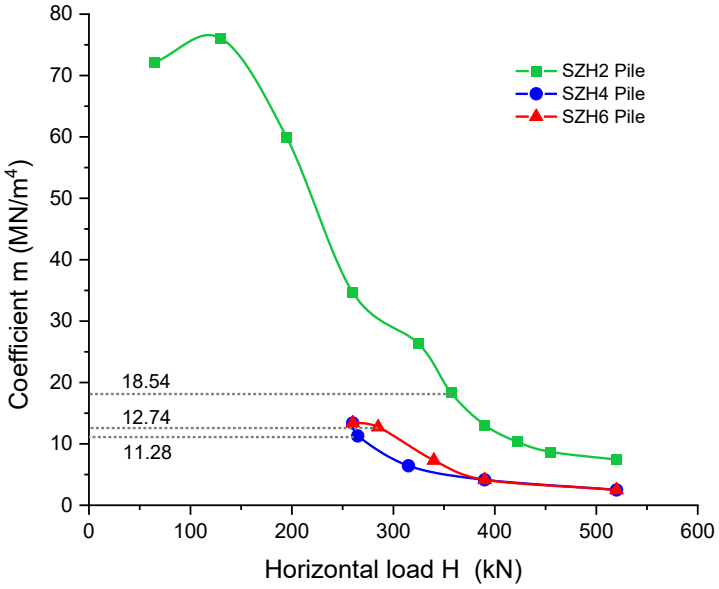

Figure 13. Variation of *m* with horizontal load for three tested piles in backfill soil.

5. Conclusions

Aim to have a sufficient comprehension of the bearing characteristics and influencing factors of rock-socketed pile foundations in deep multi-layered soft soil at backfilled nuclear power plant site, vertical and horizontal in-situ loading tests were carefully carried out. The influences of soil layers around the pile, soil layer distribution and characteristics of pile body on the bearing capacity of piles were studied. Main results and conclusions are as follows:

- Longer piles tend to have higher vertical bearing capacity, however, they do not necessarily exhibit smaller displacements when subjected to vertical load, it is also related to the distribution of soil layers and the inherent properties of the pile itself.
- When the applied vertical load increases, the effect of end resistance of piles becomes more pronounced, meanwhile, deeper soil layers exert a more significant impact on the axial forces within the pile body.
- At the vertical load level preceding failure, the distribution of axial force and shaft resistance along the pile length will change. The inhomogeneous property of the upper backfill layer may lead to significant variations in the shaft resistance along the pile.

 doi:10.20944/preprints202604.1602.v1

- The typical mechanism of transition from static to dynamic friction between soil and piles that lead to shaft resistance is more apparent for longer piles but inhomogeneous soils such as backfill and breccia layers will make the transition complex.
- For horizontal loading, piles with better integrity show more pronounced elastic features, smaller maximum horizontal displacement and less residual horizontal displacement. For long rock-socketed cast-in-place piles, further increasing the pile length has minor impact on horizontal bearing capacity, whereas the integrity of the pile body (especially the upper part integrity) influences greatly. The critical horizontal loads of piles SZH2, SZH4, SZH6 are determined to be 325kN, 260kN, 260kN, respectively. The ultimate horizontal bearing capacities of piles SZH2, SZH4 and SZH6 are all 520kN.
- The upper backfill layer has predominant influences on the horizontal bearing capacity of the piles. In theoretical method to determine horizontal bearing capacity, the selection of the proportional coefficient m should correspond to the specific load and displacement.
- For further study, we will focus on two aspects: the post-failure mechanical behavior of vertically and horizontally loaded piles, and the enhancement of bearing capacity through local artificial treatment measures, so as to provide a reference for a wider range of engineering applications.

Author Contributions: Conceptualization, L. D. and T. L.; methodology, L. D. and Lb. C.; validation, Lw. C.; formal analysis, Lw. C.; investigation, T. L.; resources, X. W.; data curation, Lb. C.; writing—original draft preparation, L. D.; writing—review and editing, T. L.; visualization, L. D.; supervision, Lw. C. and T. L.; project administration, X. W.; funding acquisition, L. D. All authors have read and agreed to the published version of the manuscript.

Funding: This research was funded by the Youth Elite Program of the China National Nuclear Corporation (grant no. KY24031), the Basic Research Project of China National Nuclear Corporation (grant no. KY26015), the Independent Scientific Reasearch Project of China Nuclear Power Engineering Co., Ltd (grant no. KY25088).

Data Availability Statement: Data are contained within the article.

Conflicts of Interest: The authors declare no conflicts of interest.

References

1. Kou, H.L.; Diao, W.Z.; Liu, T.; Yang, D.L.; Horpibulsuk, S. Field Performance of Open-Ended Prestressed High-Strength Concrete Pipe Piles Jacked into Clay. Sensors 2018, 18, 4216, doi:10.3390/s18124216.
2. Pham, T.A.; Ly, H.B.; Tran, V.Q.; Giap, L.V.; Vu, H.L.T.; Duong, H.A.T. Prediction of Pile Axial Bearing Capacity Using Artificial Neural Network and Random Forest. Applied Sciences 2020, 10, 1871, doi:10.3390/app10051871.
3. Zhang, Z.; Gong, W.; Dai, G.; Cao, X.; Zhu, Y.; Huang, H. Field Tests on Bearing Characteristics of Large-Diameter Combined Tip-and-Side Post Grouted Drilled Shafts. Applied Sciences 2021, 11, 11883, doi:10.3390/app112411883.
4. Yan, H.; Long, J.; Yang, Y.; Shi, Q.; Yang, B. Model Test Study on Bearing Characteristics of Pile Foundation in Red Clay. Buildings 2024, 14, 2316, doi:10.3390/buildings14082316.
5. Wei, Y.; Zhao, M.; Zeng, Y.; Yang, Y.; Liu, H.; Li, J.; Jie, Y. Bearing Behaviors of Rock-Socketed Piles in Layered Dynamically Compacted Soil-Rock Mixtures: A Case Study. Alexandria Engineering Journal 2025, 114, 12–29, doi:10.1016/j.aej.2024.11.087.
6. Yang, C.; Dai, G.; Gong, W.; Xi, S.; Zhu, M.; Huo, S. In Situ Study on Vertical Compressive Bearing Characteristics of Rooted Bored Piles. Buildings 2025, 15, 707, doi:10.3390/buildings15050707.
7. Bai, X.; Zhang, Y.; Yan, N.; Liu, J.; Zhang, Y. Experimental Investigation on Bearing Capacity of Rock-Socketed Bored Piles in Silty Clay Stratum in Beach Areas. Applied Ocean Research 2025, 154, 104336, doi:10.1016/j.apor.2024.104336.
8. Liu, L.; Xiao, L.; Liu, Y.; Zhao, M.; Jin, F.; Li, X.; Tian, Y. Horizontal Bearing Characteristics of Large-Diameter Rock-Socketed Rigid Pile and Flexible Pile. Buildings 2025, 15, 768, doi:10.3390/buildings15050768.

 doi:10.20944/preprints202604.1602.v1

9. Taghavi A.; Muraleetharan K.K.; Miller G.A.; Cerato A.B. Centrifuge Modeling of Laterally Loaded Pile Groups in Improved Soft Clay. Journal of Geotechnical and Geoenvironmental Engineering 2016, 142, 04015099, doi:10.1061/(ASCE)GT.1943-5606.0001443.
10. Faro V. P.; Consoli N.C.; Schnaid F.; Thomé A.; da Silva L.L. Field Tests on Laterally Loaded Rigid Piles in Cement Treated Soils. Journal of Geotechnical and Geoenvironmental Engineering 2015, 141, 06015003, doi:10.1061/(ASCE)GT.1943-5606.0001296.
11. Kang S.; Zhao Q.; Peng S.; Liu B.; Chen J. Effect of gravel-soil characters on lateral bearing capacity of pile foundation. Journal of Engineering Geology, 2019, 27(3), 559-568, doi:10.13544/j.cnki.jeg.2018-231.
12. Huang C.; Li J. Research on the influence of displacing hard shell on the horizontal bearing characteristics of pile foundation in layered soft soil. Chinese Journal of Rock Mechanics and Engineering, 2021, 40(suppl.2), 3472-3482, doi:10.13722/j.cnki.jrme.2021.0094.
13. Yang L. Research on the influence of sleeve valve pipe layered grouting technology on the horizontal bearing capacity of pile foundation in soft soil foundation. Engineering & Test, 2021, 61(3), 81-84, doi:10.3969/j. issn.1674-3407.2021.03.027.
14. Ministry of Housing and Urban-Rural Development of the People's Republic of China. Technical Code for Building Pile Foundations (JGJ 94-2008). China Architecture & Building Press, 2008.
15. Mishra A.; Sawant V.A.; Deshmukh V.B. Prediction of pile capacity of socketed piles using different approaches. Geotech Geol Eng 2019, 37, 5219-30, doi:10.1007/s10706-019-00976-0.
16. American Petroleum Institute. Recommended practice for planning, designing and constructing fixed offshore platforms. Washington: American Petroleum Institute, 2000.
17. Seol H.; Jeong S.; Kim Y. Load transfer analysis of rock-socketed drilled shafts by coupled soil resistance. Comput Geotech 2009, 36(3), 446-53, doi:10.1016/j.compgeo.2008.08.012.
18. Gutierrez-Ch J.G.; Senent S.; Melentijevic S. A DEM-based factor to design rocksocketed piles considering socket roughness. Rock Mech Rock Eng, 2021, 54, 3409-21, doi://10.1007/s00603-020-02347-1.
19. Zhang W.; Wu C.; Li Y. Assessment of pile drivability using random forest regression and multivariate adaptive regression splines. Georisk, 2021, 15(1), 27-40, doi://10.1080/17499518.2019.1674340.
20. Ministry of Housing and Urban-Rural Development of the People's Republic of China. Technical code for testing of building foundation piles (JGJ 106-2014). China Architecture & Building Press, 2014.